A SEAL TEST FACILITY FOR THE MEASUREMENT OF ISOTROPIC AND ANISOTROPIC LINEAR ROTORDYNAMIC CHARACTERISTICS

M.L. Adams and T. Yang
Case Western Reserve University
Cleveland, Ohio 44106, U.S.A.

S.E. Pace
Electric Power Research Institute
Palo Alto, California 94304, U.S.A.

A new seal test facility for measuring high-pressure seal rotordynamic characteristics has recently been made operational at Case Western Reserve University (CWRU). This work is being sponsored by the Electric Power Research Institute (EPRI). The fundamental concept embodied in this test apparatus is a double-spool-shaft spindle which permits independent control over the spin speed and the frequency of an adjustable circular vibration orbit for both forward and backward whirl. Also, the static eccentricity between the rotating and nonrotating test seal parts is easily adjustable to desired values. By accurately measuring both dynamic radial displacement and dynamic radial force signals, over a wide range of circular orbit frequency, one is able to solve for the "full" linear-anisotropic model's 12 coefficients rather than the 6 coefficients of the more restrictive isotropic linear model. Of course, one may also impose the isotropic assumption in reducing test data, thereby providing a valid qualification of which seal configurations are well represented by the isotropic model and which are not. In fact, as argued in reference [1], the requirement for maintaining a symmetric total system mass matrix means that the resulting isotropic model needs 5 coefficients and the anisotropic model needs 11 coefficients.

INTRODUCTION

The new test facility described in this paper was born out of an earlier test apparatus described in reference [2]. The earlier apparatus, while conceived and designed by the first author of this paper, was assembled by a third party in their commercial test laboratory (herein called Laboratory "X"). Basically, Laboratory "X" spent all the funds allocated for the assembly, debugging and test work without ever getting beyond the debug stage. EPRI then terminated funding this Laboratory "X" work and the hardware remnants of this unsuccessful effort remained in dormant storage at Laboratory "X" for about two years, until it was transported to CWRU in late 1985. Since then, two years have been spent redesigning certain critical portions

of the apparatus and building the new facility at CWRU. In early 1988, the test facility was ready for full system testing and the results demonstrated that the facility was capable of providing reliable test results. Consequently, this work is now moving into its next phase, i.e., testing several different seal geometries and configurations for applications in power plant centrifugal pumps. Specifically, interstage sealing annulus geometries with improved wear-resistant damping characteristics will be sought and rotordynamically quantified using this new test facility. The main body of this paper contains a brief description of the test facility, details of design changes and samples of the first group of results.

SYMBOLS

$[C_{ij}]$	damping coefficient matrix
$[D_{ij}]$	inertia coefficient matrix
$\{F_j\}$	single peak amplitudes of measured-force fundamental component
$\{f_j\}$	interactive dynamic force
R	vibration orbit radius
$[K_{ij}]$	stiffness coefficient matrix
$\{\theta_j\}$	phase angles of measured-force fundamental component
Ω	vibration orbit frequency

THE ISOTROPIC VERSUS THE ANISOTROPIC MODEL

$$\begin{Bmatrix} f_x \\ f_y \end{Bmatrix} = - \begin{bmatrix} K & k \\ -k & K \end{bmatrix} \begin{Bmatrix} x \\ y \end{Bmatrix} - \begin{bmatrix} C & c \\ -c & C \end{bmatrix} \begin{Bmatrix} \dot{x} \\ \dot{y} \end{Bmatrix} - \begin{bmatrix} D & d \\ -d & D \end{bmatrix} \begin{Bmatrix} \ddot{x} \\ \ddot{y} \end{Bmatrix} \qquad (1)$$

The isotropic model, equation (1), is now commonly used for seals for two apparent reasons. First, the isotropic model lends itself to test apparatus configurations which have already been successfully demonstrated to provide usable engineering inputs to rotor vibration analyses, e.g., the various published results of Childs, Nordmann and others. Second, the isotropic model is probably a reasonable engineering assumption for deep groove seal configurations and situations where the rotor-to-seal concentricity is accurately controlled by the bearings and other factors such as manufacturing/assembly tolerances and maintenance of highly axisymmetric temperature gradients within the overall machine and axisymmetric seal inlet pre-swirl velocity distribution.

Conversely, in dealing with the rotordynamic characteristics of fluid-film journal bearings, the strong anisotropic property stemming from journal-to-bearing eccentricity and from non-axisymmetric geometric properties has long been recognized. One might therefore expect that the more a seal resembles a journal bearing (i.e., smooth without serrations or grooves), the worse is the isotropic model approximation, and vice versa. In fact, the recently published results of Kanki and Kawakami [3] support this hypothesis. Their experimental results show a strong anisotropic effect of static eccentricity on the rotordynamic coefficients of a smooth (no grooves) seal and an almost negligible anisotropic effect of static eccentricity on the rotordynamic coefficients of a circumferentially screw-grooved seal.

The anisotropic linear model can be expressed as follows.

$$\begin{Bmatrix} f_x \\ f_y \end{Bmatrix} = - \begin{bmatrix} K_{xx} & K_{xy} \\ K_{yx} & K_{yy} \end{bmatrix} \begin{Bmatrix} x \\ y \end{Bmatrix} - \begin{bmatrix} C_{xx} & C_{xy} \\ C_{yx} & C_{yy} \end{bmatrix} \begin{Bmatrix} \dot{x} \\ \dot{y} \end{Bmatrix} - \begin{bmatrix} D_{xx} & D_{xy} \\ D_{yx} & D_{yy} \end{bmatrix} \begin{Bmatrix} \ddot{x} \\ \ddot{y} \end{Bmatrix} \qquad (2)$$

Based on arguments made in reference [1], the seal inertia matrix should be symmetric, and this translates into $d \equiv 0$ in equation (1) and $D_{xy} \equiv D_{yx}$ in equation (2).

Most of the currently operational test rigs for experimental determination of seal rotordynamic characteristics are configured to extract only the isotropic model coefficients and are correspondingly not capable of quantifying how good is the isotropic assumption for any particular seal tested, except indirectly by computing the dynamic force signals from the extracted coefficients and comparing these with the measured dynamic force signals.

To extract all the coefficients of the anisotropic model requires not only independent control over spin speed and vibration orbit frequency, but also requires a significantly two-dimensional orbit. Thus, a synchronous orbit test can not provide the necessary data to extract the anisotropic-model coefficients. Also, even with independent control over spin speed and orbit frequency, a straight-line oscillatory orbit can not provide the necessary data to extract the anisotropic-model coefficients.

It would appear that the optimum orbit to make these measurements is a circular or nearly circular orbit. The new CWRU/EPRI test apparatus described herein utilizes an independently controlled frequency and adjustable magnitude circular orbit.

DESCRIPTION OF TEST FACILITY

Overview

Various aspects of the test facility are shown in Figures 1 through 8. The conceptual schematic of the test rig spindle and seal differential pressure chamber are shown in Figure 1(a) and a layout of the original configuration, as it was first designed and built, is shown in Figure 1(b). Figure 2 shows the floor plan and elevation views of the complete test facility and Figure 3 shows the schematic of the data acquisition system. Figure 4 shows a more detailed flow chart of the data acquisition system and data reduction steps. Both the clock and trigger for the A/D conversion is external to the PC microprocessor. A 360 slot disk rotates with the orbit-frequency shaft and is used in conjunction with a fast acting optical switch to sequentially fire all data channels.

Modifications to Original Configuration

After considerable critiquing of the original test rig, two factors became obvious. First, the links for connecting the test-seal ring to the piezoelectric load measuring transducers did not sufficiently guarantee adequate axial play to insure that the hydrostatic thrust bearing maintained a non-contacting axial load support. Second, the design of the piezoelectric load measuring system relied on the concept that the primary load path (through the piezoelectric load cells) was orders of magnitude stiffer than the parallel load path through the static seals (O-rings). After extensive thought at separate solutions to these two problems, a single design solution emerged which addressed both of these problems. This design evolution is shown in Figures 5 through 8.

This final configuration has shown itself to work to the maximum satisfaction. It contains four connecting links which are relatively flexible in the axial and tangential directions but relatively quite stiff in the radial direction. The axial flexibility permits the hydrostatic thrust bearing to function as intended. The tangential flexibility nearly eliminates measurable cross-talk between the two mutually perpendicular load measuring axes. The high radial stiffness maintains the stiff load-path concept of the original design, embodying very stiff piezoelectric load cells. Finally, by making these four support links each a strain gaged transducer, they provide a second and independent measurement system for the dynamic force signals. Thus, the accuracy of the dynamic force measurements can be confirmed independently, provided both force measuring systems are simultanously working as intended. In effect, with independent dual force measuring systems, a very high degree of confidence is possible because the dual measurements are self checking. Furthermore, the addition of strain-gaged transducers permits measurement of the static radial force, which was not part of the original test rig capability.

In-Place Force System Calibrations

A linkage has been designed which attaches to the exposed closure bolt circle when the front closure head is removed. It allows a known force to be applied directly to the test seal ring, in any of the multitude of radial directions of the bold circle holes. A schematic of this calibration system is shown in Figure 9. Both force measuring systems are simultaneously calibrated with this setup. It is quite easy and quick to use, thus allowing frequent recalibration, such as at the beginning and end of each test sequence, if desired. Actually, both force measuring systems are quite stable and do not require such frequent recalibration.

FIRST TEST RESULTS OBTAINED (JANUARY 1988)

Figures 10 through 13 show typical measurement output samples. Figure 10 shows a cycle of force output, time averaged over only two cycles, whereas Figure 11 shows the same case time averaged over 20 cycles. Figures 10 through 12 are from the F_X load axis piezoelectric measurements. Figure 12 shows the fundamental Fourier series component (i.e., Ω), which is the portion of the signal that is utilized in extraction of the rotordynamic coefficients. Figure 13 shows a superposition of the same F_X signal fundamental component extracted simultaneously from the independent strain-gage system and the piezoelectric system.

In making the comparison of signals shown in Figure 13, it is important to know that the seal tested was a deep groove labyrinth configuration with only a 50 psi pressure drop through it. Also, it was a concentric orbit, i.e., nominally a zero static eccentricity. The dynamic eccentricity (orbit radius) was only 1.3 mils. Consequently, the force signals were quite small (10 lb. maximum) which was intentionally devised in order to subject the two independent force measuring systems to a most stringent comparison test. With the present load measuring links, the peak dynamic load capability is approximately 700 lbs, being set by the strain-gaged links' strength limitation. The Kistler piezoelectric system has a much higher maximum load limitation. We believe these results indicate that the test rig is capable of making reliable measurements of rotordynamic characteristics.

Table 1 summarizes the data-reduction simultanous equations for a circular orbit. Table 2 shows a sample of reduced data, comparing the two sets of rotordynamic coefficients derived from the two independent force measuring systems. It is important to bear in mind when evaluating these initial results that the dynamic forces were quite small.

CONCLUDING REMARKS

The CWRU/EPRI seal rotordynamic test facility described in this paper is now operational and all indications are that it provides reliable test data. It provides the anisotropic coefficients and thus provides a valid qualification on the validity of the isotropic model for any seal tested. The addition of a strain-gage based back-up force measuring system provides independent self-checking capability and the additional feature of measuring the static load components in addition to the dynamic load signals. Also, the adjustable static eccentricity and dynamic eccentricity (0 to 0.060 inches) allows testing to determine limits of the linear model's validity as vibration orbit magnitude is increased. Furthermore, in addition to making accurate determination of seal rotodynamic coefficients, this facility will be used to make fundamental investigations into the validity of the basic mechanical impedance hypothesis as it is now taken for granted by most investigators. These are fundamental investigations related to topics recently reviewed in reference [1].

REFERENCES

1. Adams, M.L.: Insights Into Linearized Rotor Dynamics, Part 2. Journal of Sound and Vibration, Vol. 112(1), 1987, pp. 97-110.

2. Adams, M.L. and Makay, E.: Development of Advanced Rotor-Bearing Systems for Feedwater Pumps - Phase III: Hardware Design and Fabrication. EPRI Final Report CS-3203, July 1983.

3. Kanki, H. and Kawakami, T.: Experimental Study on the Static and Dynamic Characteristics of Screw Grooved Seals. Proceedings, ASME Rotating Machinery Dynamics papers, ASME 11th Biennial Conference on Mechanical Vibration and Noise, Boston, Sept. 27-30, 1987, DE-Vol. 2, pp. 273-278.

$$(F_x \cos\theta_x) / R = -K_{xx} - \Omega_J C_{xy} + \Omega_J^2 D_{xx}$$

$$(F_x \sin\theta_x) / R = K_{xy} - \Omega_J C_{xx} - \Omega_J^2 D_{xy}$$

$$(F_y \cos\theta_y) / R = -K_{yx} - \Omega_J C_{yy} + \Omega_J^2 D_{yx}$$

$$(F_y \sin\theta_y) / R = K_{yy} - \Omega_J C_{yx} - \Omega_J^2 D_{yy}$$

$$J = 1, 2, 3$$

Table 1. Simultaneous coefficient-extraction equations for a circular orbit.

Kk LB/INCH

2878	1838
-2351	2654

Ks LB/INCH

2106	1954
-2172	1870

Ck LB*SEC/INCH

67.51	11.93
-10.87	76.35

Cs LB*SEC/INCH

57.42	16.34
-9.480	66.45

Dk LB*SEC*SEC/INCH

4.941E-2	-1.055E-1
1.332E-1	3.948E-2

Ds LB*SEC*SEC/LB

5.523E-2	-9.479E-2
1.213E-1	3.788E-2

SHAFT SPEED = 1500 RPM

ORBIT FREQ. = 676, 1446, 1952 RPM

ORBIT RADIUS = 1.40 MIL

Table 2. Sample rotordynamic coefficients, comparing results from piezoelectric measurements with results from strain gage measurements.

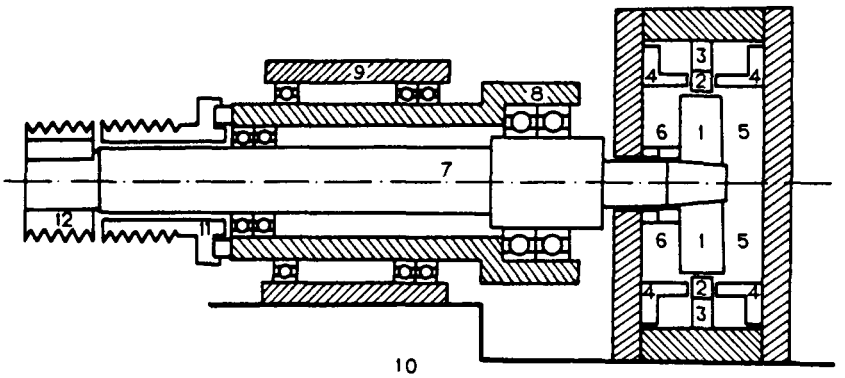

1 - Test rotating element
2 - Test annulus ring
3 - Piezoelectric load cells
4 - Hydrostatic axial ring supports
5 - High-pressure compartment
6 - Low-pressure compartment
7 - Inner spindle rotor
8 - Outer spindle rotor
9 - Spindle housing
10 - Support base
11 - V-belt pulley
12 - V-belt pulley

1(a) Conceptual Sketch of Rotor Support Component Test Apparatus

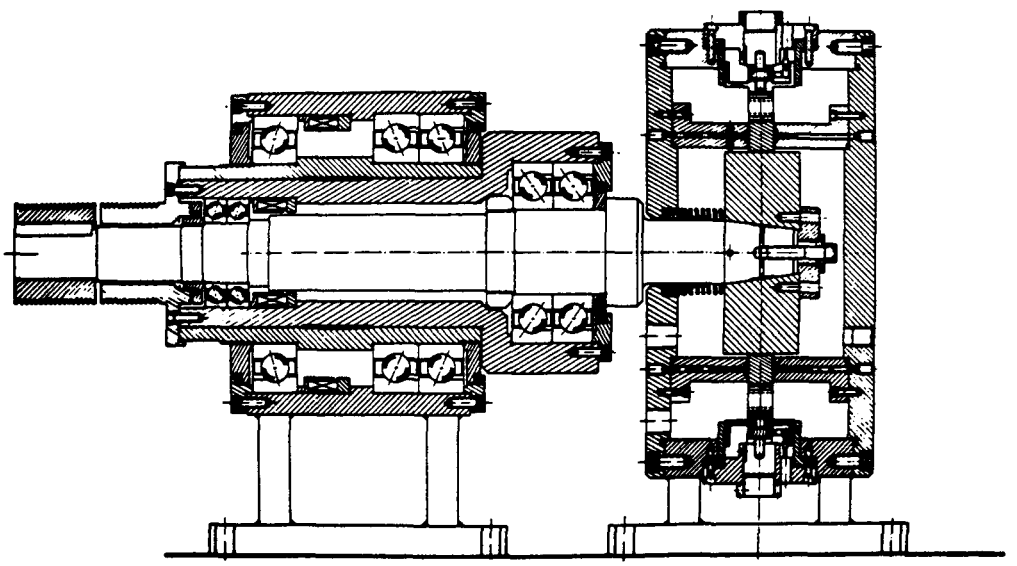

1(b) Assembly Layout of Rotor Support Component Test Apparatus

Figure 1. Test Apparatus, Reference (3)

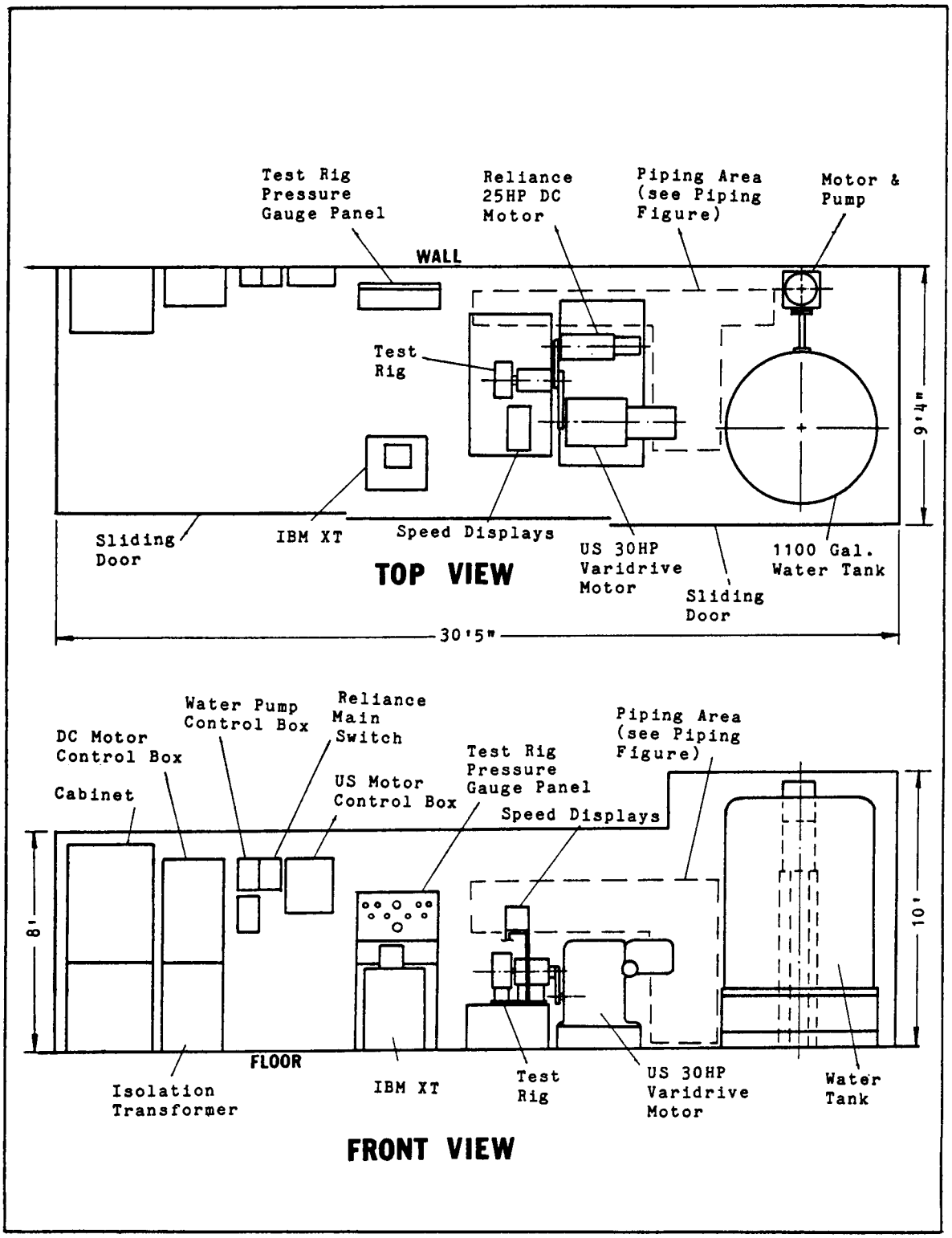

Fig. 2. Floor plan and elevation view of test facility.

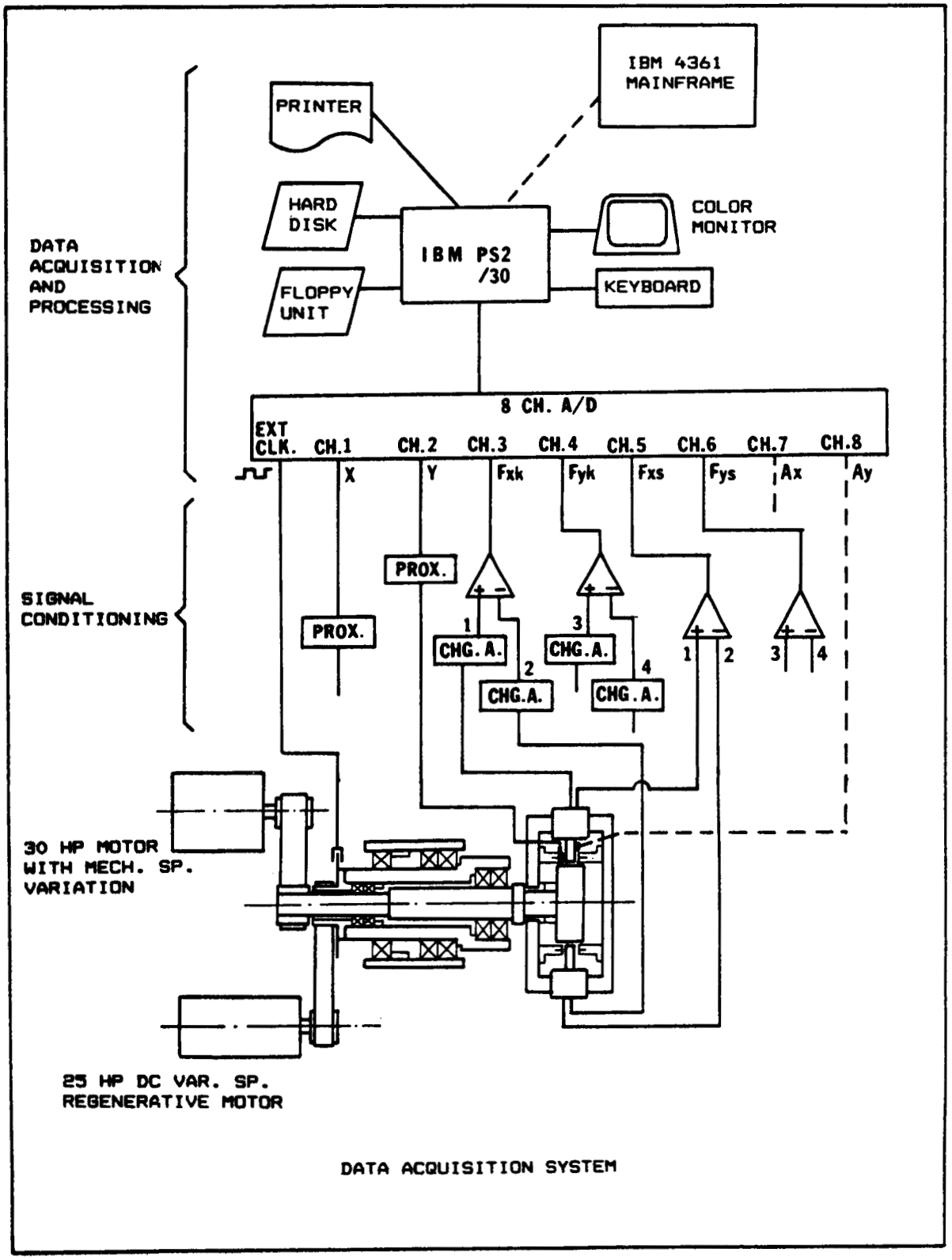

Fig. 3. Schematic of data acquisition system.

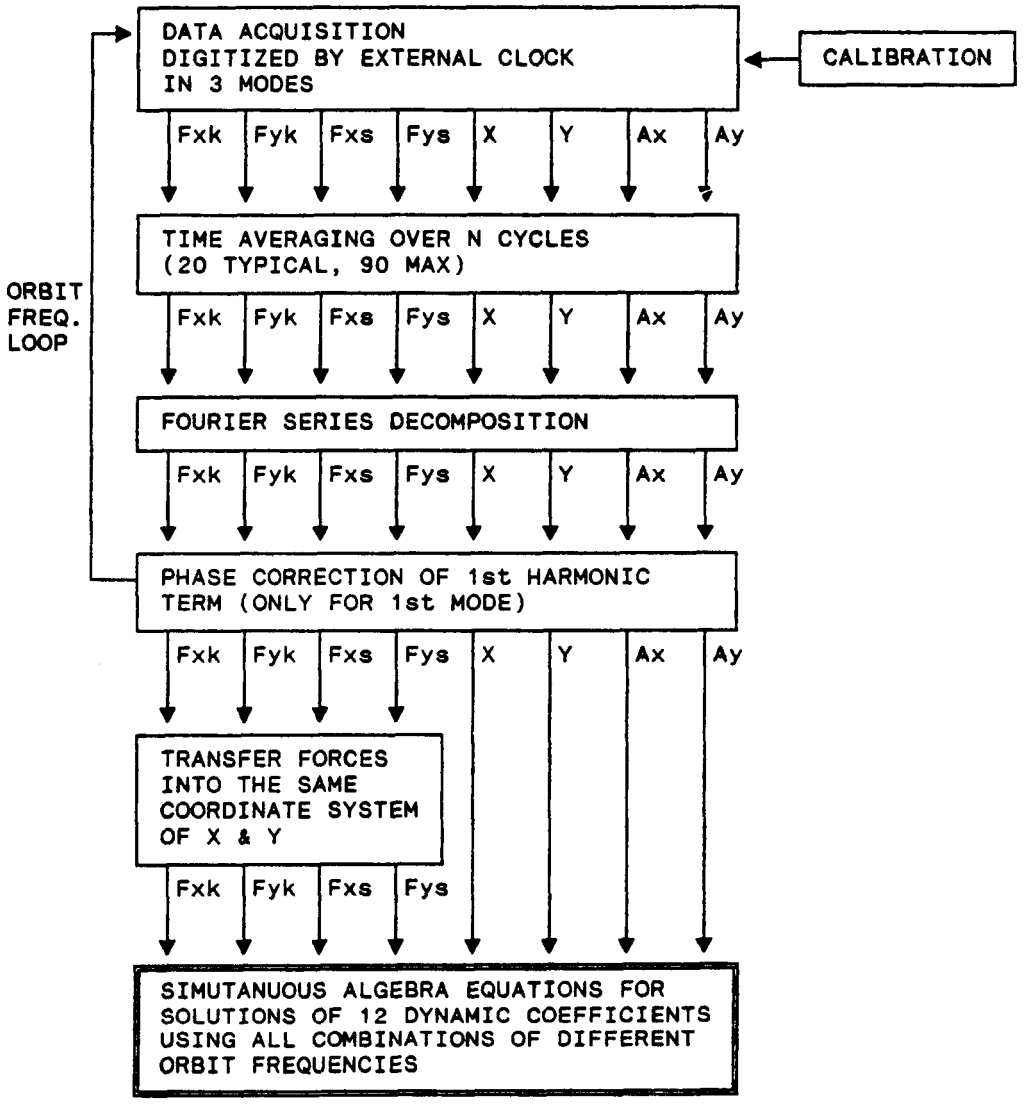

Fig. 4. Data acquisition and analysis overview.

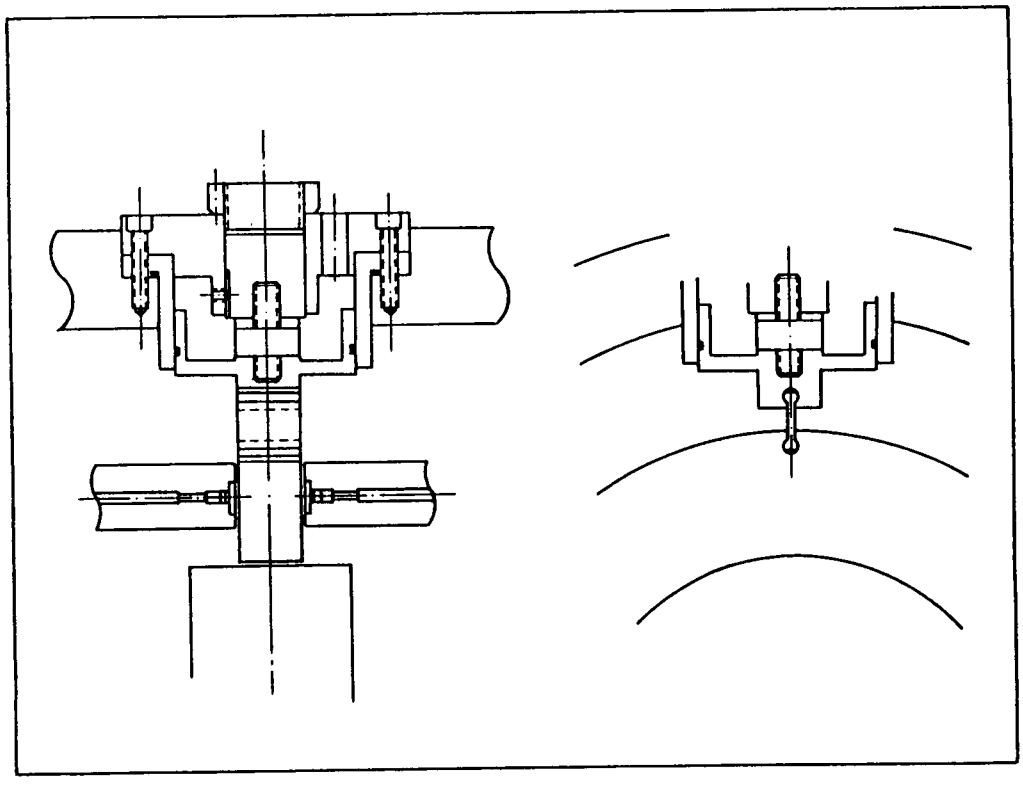

Fig. 5. Original load measuring and support system.

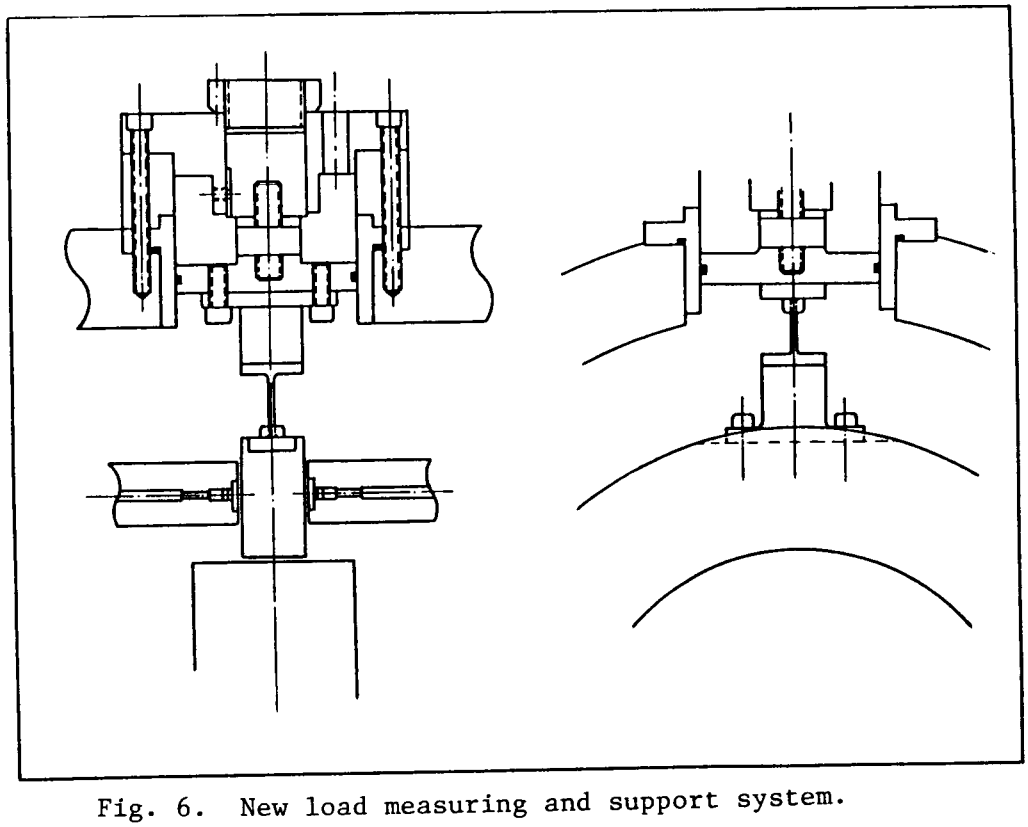

Fig. 6. New load measuring and support system.

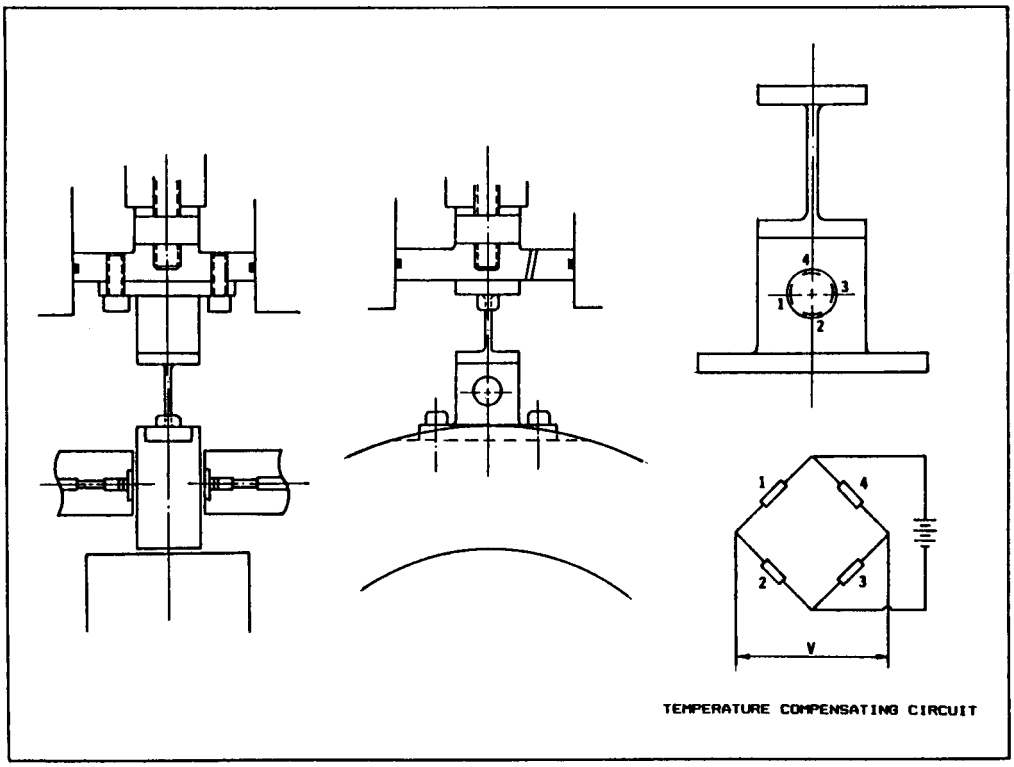

Fig. 7. New load measuring and support system with strain gage transducer.

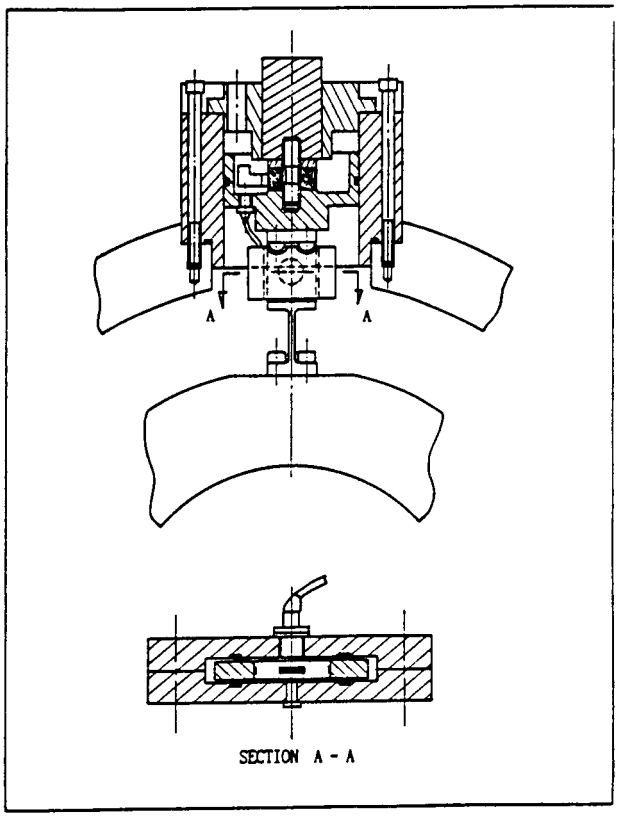

Fig. 8. New load measuring system, showing complete assembly with water-seal barrier.

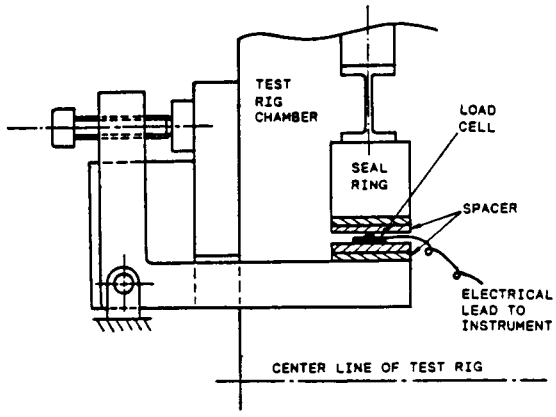

Fig. 9. In-place load calibration system.

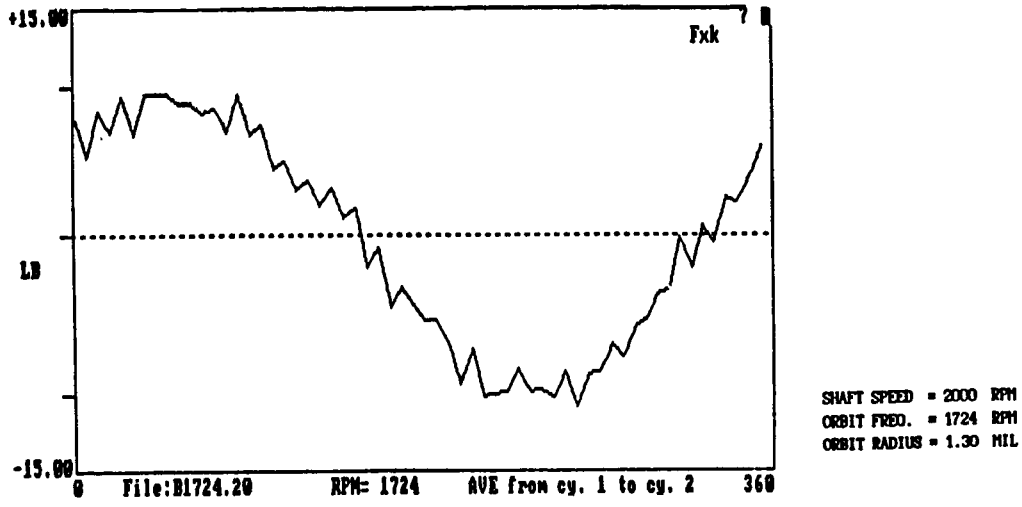

Fig. 10. Sample measurement, time averaged over 2 cycles.

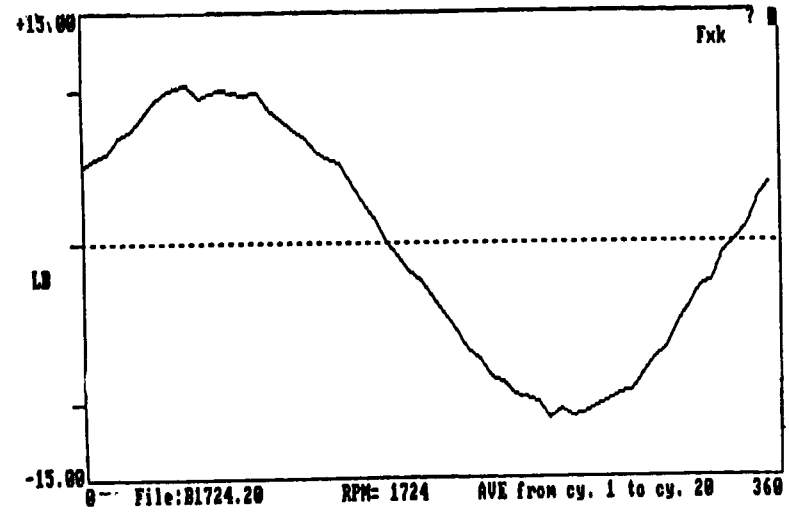

Fig. 11. Sample as in Figure 10, but time averaged over 20 cycles.

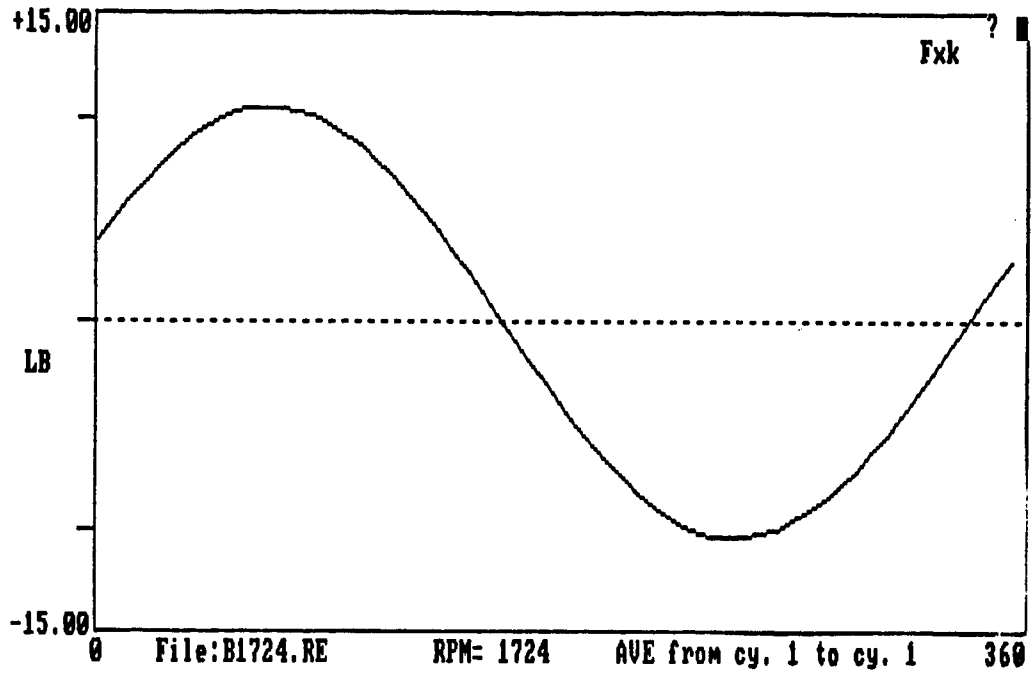

Fig. 12. The fundamental (Ω) frequency component from time-averaged signal given in Figure 11.

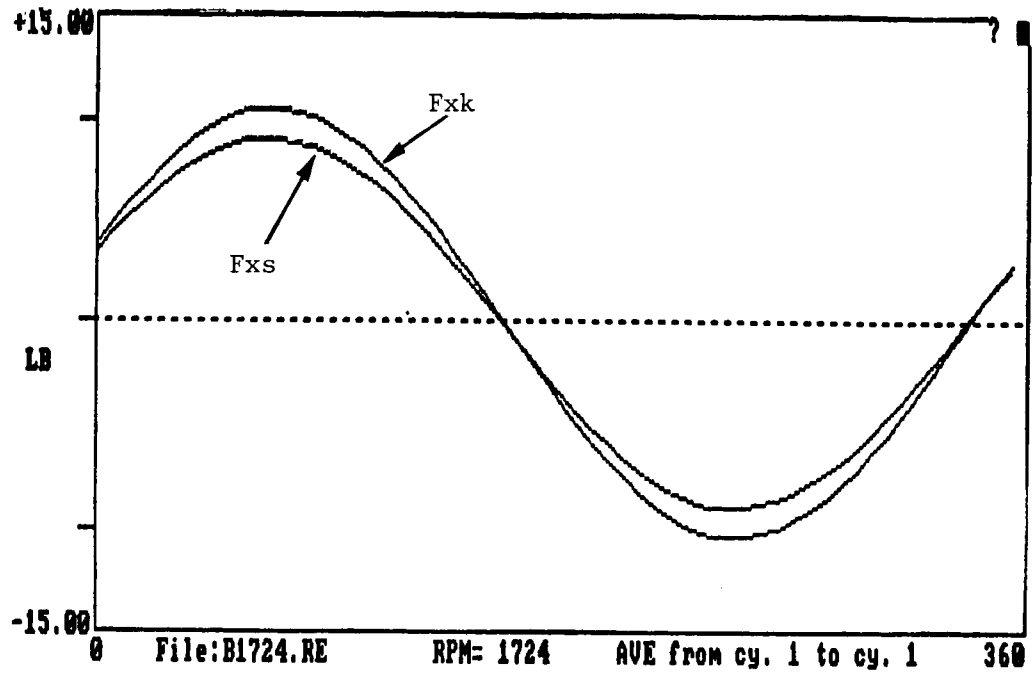

Fig. 13. Comparison of fundamental (Ω) frequency component measured simultaneously with both force measuring systems.